Journal of Structural Engineering & Applied Mechanics (2025) 8(4):246-260
DOI 10.31462/jseam.2025.04246260

RESEARCH ARTICLE

Preliminary design-based assessment of lead rubber bearing isolation systems in Türkiye considering soil classes and seismic hazard

Seda Öncü-Davas[1*]

[1] Istanbul University-Cerrahpasa, Department of Civil Engineering, Istanbul, Türkiye

Article History

Received 12 October 2025
Accepted 29 November 2025

Keywords

Seismic isolation
Lead rubber bearing
Soil class
Turkish Earthquake Hazard Map
Preliminary design parameter

Abstract

Türkiye is located in a region of high seismic hazard due to the dense distribution of active fault lines. Major earthquakes that have occurred in the country, particularly the 1999 Kocaeli and 2023 Kahramanmaraş events, have demonstrated not only the devastating potential for loss of life but also the critical importance of maintaining the functional performance of buildings after seismic events. In this context, seismic isolation systems, which extend the building period to reduce earthquake forces and dissipate energy at the isolation level, have gained increasing attention and application in recent years. However, the design parameters of such systems vary depending on the local soil class, seismic intensity level, and geographical coordinates. In this study, a preliminary design of lead rubber bearings (LRBs) was conducted for a typical five-story reinforced concrete building using the data provided by the Turkish Earthquake Hazard Map (TDTH). For each soil class (ZA, ZB, ZC, and ZD), preliminary design results were obtained across all geographical coordinates in the TDTH and subsequently transferred to a GIS-based QGIS environment. The spatial distributions of isolator diameter and base displacement demands were mapped, and these parameters, together with the effective period, characteristic strength ratio, and effective damping ratio, were statistically evaluated to identify regional trends under different soil conditions. Accordingly, this study provides engineers and practitioners with an order-of-magnitude assessment of how soil class influences the preliminary design parameters of seismic isolation systems across Türkiye, based on a representative five-story building equipped with lead rubber bearings, through both statistical and geospatial analyses.

1. Introduction

Türkiye is located in an active seismic zone characterized by a dense network of fault lines, which has always made the seismic safety of buildings one of the most critical engineering challenges. The 1999 Kocaeli earthquake, with a moment magnitude of 7.6 (Mw 7.6), caused approximately 17,000 casualties, severe economic losses, and extensive damage to the existing building stock. Similarly, the 2011 Van earthquake (Mw 7.1) resulted in significant destruction and loss of life. Most recently, the Mw 7.8 Pazarcık and Mw 7.5 Elbistan earthquakes that struck Kahramanmaraş on February 6, 2023, led to the deaths of more than 50,000 people and rendered hundreds of thousands of buildings uninhabitable. These major earthquakes have once again revealed the seismic hazard reality of Türkiye and the urgent need for advanced engineering solutions

[*] Corresponding author (seda.oncu@iuc.edu.tr)
eISSN 2630-5763

to ensure building safety. The Pazarcık and Elbistan earthquakes have clearly demonstrated that ensuring life safety alone is not sufficient; the uninterrupted functionality of hospitals, public buildings, and industrial facilities is also of vital importance for the resilience of cities [1]. In this context, seismic isolation technology stands out as one of the most effective solutions, enabling the protection of both buildings and their contents [2, 3]. These systems, which reduce earthquake forces by lengthening the building period and dissipating energy at the isolation level, have been increasingly implemented both worldwide and in Türkiye [4, 5]. Thanks to seismic isolation, the superstructure moves almost as a rigid box, leading to a significant simultaneous reduction in interstory drifts and floor accelerations. In this way, both structural and nonstructural components are protected, and the building contents are effectively safeguarded from the damaging effects of earthquakes [6, 7]. In Türkiye, in accordance with the directive of the Ministry of Health, many city hospitals have been constructed with seismic isolation systems over the past decade. Among these are some of the largest base-isolated healthcare facilities in the world, such as the Istanbul Çam and Sakura City Hospital (2068 isolators), the Adana City Hospital (1552 isolators), and the Isparta City Hospital (903 isolators) [4, 8, 9]. In addition, other major structures, including the approach viaducts of the 1915 Çanakkale Bridge, several airport terminals in Istanbul, and the historic Göztepe Train Station, have also been designed or retrofitted using seismic isolation technology [10]. These examples demonstrate that seismic isolation has become a successfully implemented engineering solution for various building types in Türkiye. In this context, with the growing awareness of its effectiveness, the demand for seismic isolation technology has also increased in residential buildings, and its applications have been gradually expanding in this field.

The Turkish Building Earthquake Code (TBEC-2018) [11] introduced, for the first time, detailed provisions for the design of seismic isolation systems in Chapter 14, enabling the reliable, standardized, and controllable design of base-isolated buildings. The code provides comprehensive explanations regarding the preliminary design, analysis methods, and performance objectives of isolation systems. However, in the analysis procedures specified in TBEC-2018 for defining the effects of earthquake ground motions on buildings, it is observed that the spectral values obtained from the national earthquake hazard map are primarily used. The Turkish Earthquake Hazard Map was developed based on ground motion prediction models that consider the seismic potential of active faults, magnitude recurrence relationships, horizontal distance from the surface projection of fault ruptures, and source mechanisms. Within this framework, the spectral parameters provided by the Turkish Earthquake Hazard Map are defined based on soil class, seismic intensity level, and geographical coordinates. Therefore, spectral parameters that depend on soil class emerge as a key factor directly influencing the performance of seismically isolated systems. This relationship has also been confirmed by several studies in the literature investigating the critical role of soil conditions in isolation effectiveness. Castaldo and Ripani [12] reported that isolation systems perform more effectively and predictably on stiff and medium-stiff soils, while soft soils, due to their low-frequency motion characteristics, tend to cause resonance effects that reduce isolation performance. Similarly, Hassan and Pal [13] found that stiff and medium-stiff soils provide the most favorable conditions for base isolation, whereas on soft soils, spectral acceleration, displacement, and interstory drift demands increase significantly, leading to reduced isolation efficiency. Studies that also consider near-fault and far-fault effects have shown that isolation systems experience higher acceleration, displacement, and base shear demands on soft soils, resulting in more pronounced performance degradation under these conditions [14, 15]. In terms of soil-structure interaction, Yanik and Ulus [16] demonstrated that the effectiveness of seismic isolation systems decreases particularly in soft soils. Moreover, Ghosh and Das [17], through analyses conducted under both near-fault and far-fault ground motions for different soil conditions, showed that soil-structure interaction in soft soils limits the acceleration reduction capacity of seismic isolation and increases base displacements, especially under near-fault effects.

However, most of the existing studies have mainly focused on analyses that consider soil classes for specific scenario earthquakes or a limited number of geographical coordinates. It is still important to conduct comprehensive studies that systematically present preliminary design parameters of seismic isolation systems for different soil classes based on the data of the Turkish Earthquake Hazard Map. In this study, the preliminary design of a seismic isolation system composed of lead rubber bearings (LRBs) for a typical five-story reinforced concrete building was carried out by considering different soil classes for all coordinates available in the Turkish Earthquake Hazard Map (TDTH) platform of AFAD [18]. The main objective is to provide engineers and practitioners with map-based preliminary information and an order-of-magnitude evaluation regarding isolation system design parameters. Spectral parameters obtained from the TDTH database, namely the spectral accelerations for short periods (S_S) and for a period of 1.0 s (S_1), were used for the DD-1 earthquake level, which represents the design level adopted for the isolation system and the substructure of seismically isolated buildings in accordance with the Turkish Building Earthquake Code (TBEC-2018). These data were integrated into a preliminary design code developed in MATLAB [19], and the results were generated for each coordinate. The preliminary design outcomes obtained separately for each coordinate and soil class on the Turkish Earthquake Hazard Map were then transferred to a GIS-based QGIS environment [20], where the spatial distributions of isolator diameter and base displacement demands were mapped. In addition, key design parameters such as base displacement (D_m), isolator diameter (B), effective period (T_{eff}), characteristic strength ratio (F_Q/W) and effective damping ratio (β_{eff}) were statistically evaluated to reveal regional and statistical trends of the isolation system performance under different soil conditions.

The present study was conducted within the scope of preliminary design and is therefore limited to a representative five-story reinforced concrete building equipped with lead rubber bearings (LRBs). To focus on developing a generalizable preliminary design framework rather than assessing detailed structural responses, nonlinear time-history and modal response spectrum analyses, as well as near-fault ground motion effects, were deliberately excluded from the scope.

2. Methodology for preliminary isolator design

In this study, the preliminary design calculations of a building's isolation system were performed using a code developed in the MATLAB [19] environment. The steps of the calculation process are as follows:

Step 1. Definition of building properties. The number of stories, the number of spans in both directions, the soil class, the seismic hazard level, and the design limits of the isolation system were defined as user inputs. In this study, a five-story building model (excluding the isolation level) with five spans in both the X and Y directions and a span length of 5 m was considered as a representative example. The dead load was assumed as G = 1.2 t/m² and the live load as Q = 0.2 t/m². Using these values, the floor area, total dead and live loads, and the seismic weight of the building (W = G + nQ) were calculated. The total building weight was distributed among the isolators according to the column layout to obtain the axial load per isolator. This value was then multiplied by a factor of 1.1 to represent the higher axial load level in the central columns, and the maximum axial load (P_{max}) was determined accordingly.

Step 2. Determination of earthquake parameters. Coordinate-based spectral acceleration coefficients (S_S, S_1) obtained from the Turkish Earthquake Hazard Map (TDTH) platform of AFAD [18] were integrated into the code. For the user-defined earthquake hazard level and soil class, the design spectral acceleration coefficients (S_{DS}, S_{D1}) were calculated using the local site coefficients (F_S, F_1) specified in TBEC-2018.

Step 3. Preliminary design of the isolation system. In TBEC-2018, the analysis methods that can be used in the earthquake design of the superstructure and substructure of seismically isolated buildings are defined. Within this scope, the Equivalent Lateral Force Method, the modal combination method, and the linear time history analysis method can be applied depending on the conditions specified in the code. In this study, the

Equivalent Lateral Force Method was adopted for the preliminary design of the lead-core rubber bearing isolation system.

The parameters of lead rubber bearings (LRBs) defined in the catalog of the manufacturer [21] were considered. During the isolator selection process, the isolator diameter (B) was first chosen according to the maximum axial load (P_{max}) acting on the isolator. Then, it was ensured that the base displacement demand (D_m) obtained from the iterations did not exceed the displacement capacity (D_{max}) specified in the catalog. If the displacement demand exceeded the capacity, a larger isolator diameter was selected. The lead core placed at the center of the lead rubber bearing provides energy dissipation and contributes to reducing the horizontal displacements of the seismic isolation system. The lead core diameter is typically between one-sixth and one-third of the total isolator diameter [22]. To achieve a higher damping capacity, the lead core diameter was defined as one-sixth of the outer diameter ($B_L = B/6$). The core area was calculated based on the core diameter using the expression $A_P = \pi {B_L}^2/4$, and the characteristic strength (F_Q) was determined according to Eq. (1), depending on this area. The yield shear stress of the lead material was taken as τ_{pb}= 10 MPa. The post-yield stiffness of the isolator (k_2) was calculated according to Eq. (2), considering the rubber area around the lead core ($A_r = \pi(B - B_L^2)/4$), the shear modulus of rubber (G_v = 0.4 MPa), and the total rubber thickness (T_r). The total rubber thickness was initially assumed as T_r = 300 mm. However, in cases where the shear strain limit is defined in TBEC-2018 ($D_m/T_r \leq 2$) was not satisfied, the T_r value was increased by 10 mm at each iteration until the condition was met. The shape factor (S) was calculated using Eq. (3), assuming a single rubber layer thickness of t = 9 mm. The elastic modulus of the rubber material was taken as $E_0 = 4G_v$. The compression modulus (E_c), vertical stiffness modulus (E_v), and vertical stiffness (k_v) of the isolation unit was then computed using Eq. (4)-(6), respectively. The bulk modulus of the rubber material was taken as K = 2000 MPa, and the rubber hardness coefficient as k =0.6. The hysteretic behavior of the lead rubber bearing was represented by a bilinear model. In this model, the pre-yield stiffness was calculated as $k_1 = k_2/\alpha$, where α = 0.1 is the ratio of post-yield to pre-yield stiffness. The yield displacement (D_y) and equivalent stiffness (k_e) of each isolator was calculated using Eq. (7) and (8). The effective period of the isolation system (T_{eff}) was determined from the total effective stiffness (K_e) using Eq. (9), while the effective damping ratio (β_{eff}) and the damping modification factor (η) were computed using Eq. (10) and (11). The seismic hazard level used in the preliminary design phase could be selected by the user. In this phase, the characteristic strength (F_Q) and post-yield stiffness (k_2) values were updated by multiplying by the lower and upper limit ($\lambda F_{q,lower} = 0.595$, $\lambda F_{q,upper} = 1.607$, $\lambda k_{2,lower} = 0.765$, $\lambda k_{2,upper}$ =1.832). Thus, all preliminary design parameters varied depending on these limits. Since this study aims to present the base displacement and related parameters calculated within the scope of the Equivalent Lateral Force Method defined in TBEC-2018, the calculations were performed for the DD-1 earthquake level using the lower limit assumptions. For the DD-1 level, which corresponds to the most severe earthquake hazard, the base displacement was calculated according to Eq. (12), considering the spectral acceleration value corresponding to the effective period of the isolation system ($S_{ae}(T_{eff})$) and the damping modification factor (η). To account for torsional effects, the base displacement demand was increased by 10%. Mathematical definitions of the mechanical parameters of the LRB system are given in Table 1. Fig. 1 presents the flowchart of the preliminary design procedure developed in MATLAB for selecting the LRB parameters according to the Equivalent Lateral Force Method defined in TBEC-2018.

Step 4. Evaluation of results. The isolator diameter and base displacement demands obtained from the preliminary design results, which were performed separately for each coordinate and soil class on the Turkish Earthquake Hazard Map [18], were transferred to GIS-based analyses and mapped using the QGIS program [20]. In addition, other parameters such as base displacement, effective period, characteristic strength ratio, and effective damping ratio were statistically presented for each soil class. In this way, both the regional and statistical distributions of the isolator design parameters under different soil conditions were revealed.

Table 1. Mechanical parameters for the LRB base-isolation system

Parameter	Mathematical definition	
Characteristic strength	$F_Q = A_p \tau_{pb}$	(1)
Post-yield stiffness	$k_2 = G_v \left(\frac{A_r}{T_r}\right)$	(2)
Shape factor	$S = (B^2 - B_L^2)/4Bt$	(3)
Compression modulus of the isolation unit	$E_c = E_0(1 + 2kS^2)$	(4)
Vertical stiffness modulus	$E_v = \frac{1}{\frac{1}{E_c} + \frac{1}{K}}$	(5)
Vertical stiffness	$k_v = \frac{E_v A_r}{T_r}$	(6)
Yield displacement	$D_y = \frac{F_Q}{(k_2 - k_1)}$	(7)
Effective stiffness	$k_e = k_2 + \frac{F_Q}{D}$	(8)
Effective isolation period	$T_{eff} = 2\pi \sqrt{\frac{W}{K_e g}}$	(9)
Effective damping ratio	$\beta_{eff} = \frac{2Q(D - D_y)}{\pi K_e D^2}$	(10)
Damping reduction factor	$\eta = \sqrt{\frac{10}{5 + \beta_{eff}}}$	(11)
Base displacement	$D_m = 1.3\left(\frac{g}{4\pi^2}\right) T_{eff}^2 \eta S_{ae}(T_{eff})$	(12)

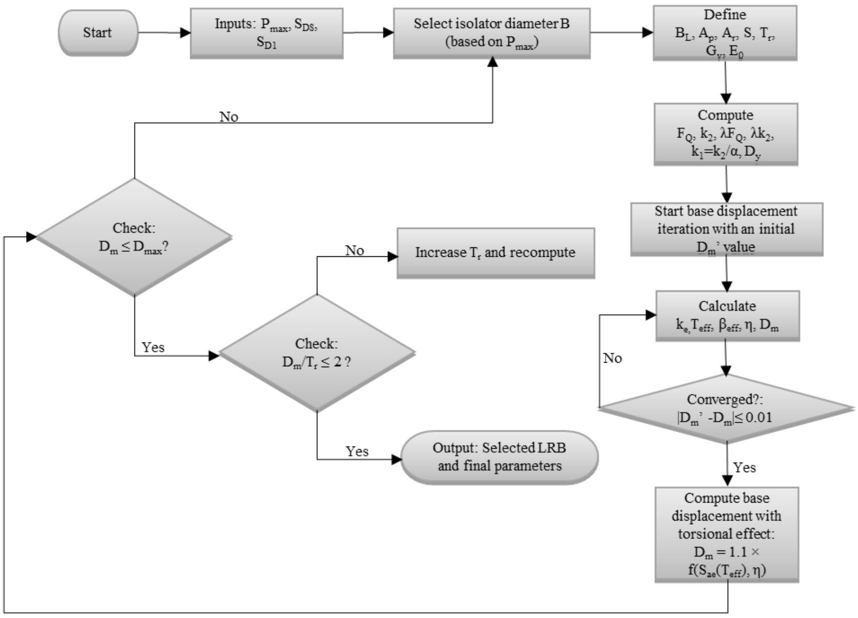

Fig. 1. Flowchart of the preliminary design procedure of the LRB isolation system according to the TBEC-2018 Equivalent Lateral Force Method

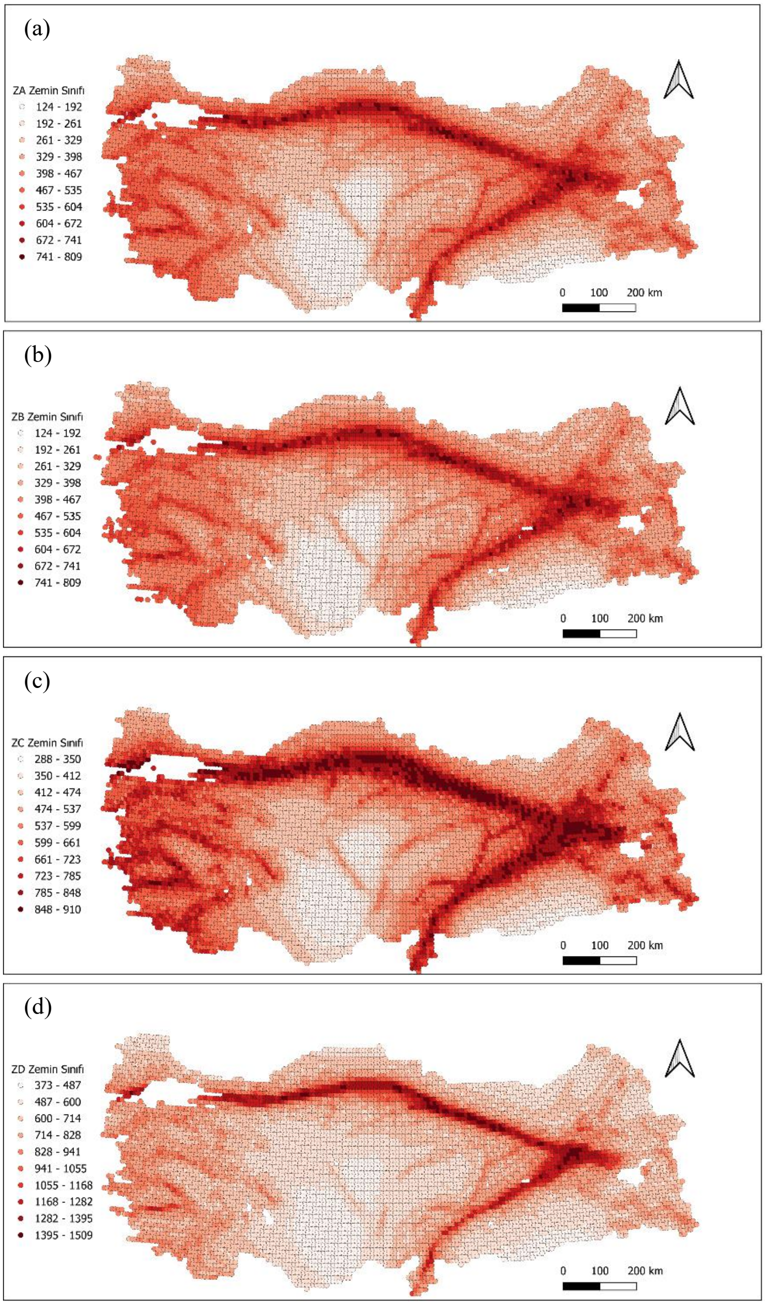

Fig. 2. Distribution of base displacement (D_m) demands by soil class for a five-story reinforced concrete building equipped with lead rubber bearings: a) ZA, b) ZB, c) ZC, d) ZD

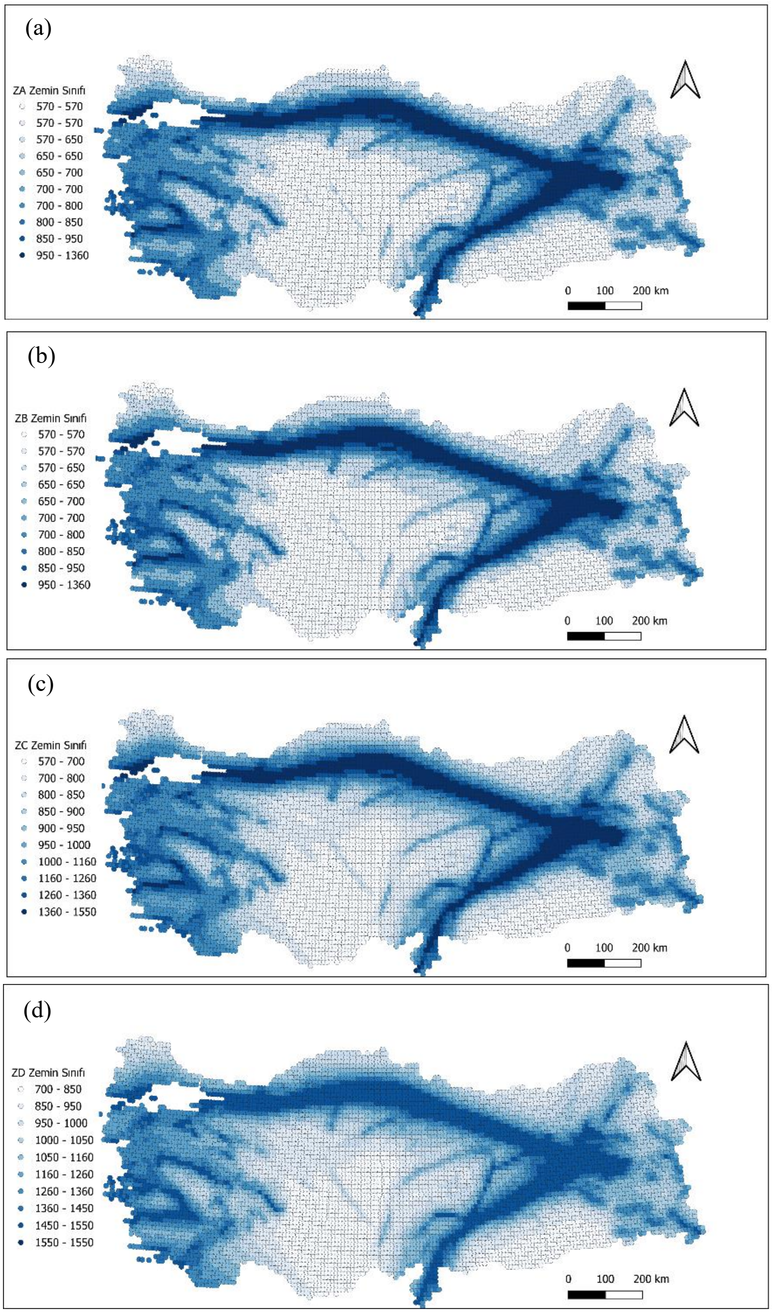

Fig. 3. Distribution of isolator diameters (B) by soil class for a five-story reinforced concrete building equipped with lead rubber bearings: a) ZA, b) ZB, c) ZC, d) ZD

Fig. 2 presents the distribution of base displacement demands obtained for different soil classes (ZA, ZB, ZC, and ZD) across Türkiye, based on the preliminary design calculations for a five-story reinforced concrete building equipped with lead rubber bearings. According to TBEC-2018, the local site coefficient for a period of 1.0 s (F_1) and the spectral acceleration coefficient (S_1) are equal for soil classes ZA and ZB. Therefore, the design spectral acceleration coefficient (S_{D1}) is also identical for these two soil classes. Since the effective period (T_{eff}) used in the calculation of base displacement demands lies in the long-period range, the computations are performed using the long-period coefficient (S_{D1}). Consequently, both the base displacement demands and all related design parameters are the same for ZA and ZB soil classes. When the maps are examined, it is observed that the base displacement demands are relatively low in stiff and very stiff soils (ZC and ZD) and in rock-type soils such as ZA and ZB. However, higher base displacement demands are concentrated along the North Anatolian and East Anatolian fault zones. As soil stiffness decreases (from ZC to ZD), both the displacement demands increase, and these effects spread over a wider geographical area. Particularly for the ZD class, base displacement demands exceeding 1.0 m appear in certain fault zone regions. Such displacement levels are difficult to accommodate within the physical capacity limits of the isolators. Moreover, the need for significantly larger isolator sizes and wider structural seismic gaps introduces serious engineering challenges in practical applications. Fig. 3 illustrates the distribution of isolator diameters for a five-story reinforced concrete building equipped with lead rubber bearings across Türkiye, depending on soil class. For soil classes ZA and ZB, the isolator diameters range between 570 mm and 1360 mm, while for ZC they vary between 570 mm and 1550 mm, and for ZD between 700 mm and 1550 mm. This indicates that even in rock-type soils, large isolator diameters may be required at certain locations, particularly near active fault zones. As soil stiffness decreases, the required isolator diameter increases both in magnitude and in spatial extent, making the design process more challenging.

Based on the TDTH parameter values, the distribution of maximum base displacement (D_m) obtained for all coordinates across Türkiye is presented in Fig. 4(a) as box plots for each soil class. In rock-type soils (ZA and ZB), the minimum and maximum base displacement demands range from 124 mm to 809 mm, with median values around 400 mm. Since the interquartile range (IQR), which represents the spread of the middle 50% of the data, is relatively small, it indicates that base displacement demands in firm soils are not only relatively low but also occur within a narrow range. Although the outliers, representing exceptional base displacement cases, are concentrated around the upper limit of approximately 800 mm, these points do not reflect the typical characteristics of the distribution. In stiff soils (ZC), the median base displacement demand increases to 566 mm, with minimum and maximum values of 288 mm and 910 mm, respectively. The increase in the IQR also indicates that both the average displacement demand and its variability have increased. For soft soils (ZD), the highest base displacement demands are observed. The median value is 670 mm, while the minimum and maximum values are 373 mm and 1509 mm, respectively. The upper adjacent value is 1059 mm, and 559 of the total 8116 coordinate points are identified as finite outliers, ranging between 1059 mm and 1510 mm. These results show that seismically isolated buildings located in ZD soil zones are subjected to excessive base displacement demands, and the extreme values observed around fault zones pose significant challenges for engineering design.

In Fig. 4(b), the statistical distributions of isolator diameter (B) values for different soil classes are presented in boxplot format. For soil classes ZA and ZB, the median isolator diameter is 700 mm, with relatively narrow distribution ranges and upper adjacent values around 1050 mm. In these classes, the minimum and maximum isolator diameters are 570 mm and 1360 mm, respectively. It was observed that the isolator diameter requirements exceeded the upper adjacent values for 373 of the 8116 coordinates, identified as finite outliers. This indicates that isolator sizes are generally smaller in rock-type soils, although significantly larger diameters may be required in areas of high seismic hazard near active fault zones. In stiff soils (ZC), the median diameter increases to 950 mm, the box height becomes wider, and the upper adjacent value reaches 1550 mm. This increase shows that higher displacement capacities must be accounted for in isolator design for the ZC soil class. For soft soils (ZD), the isolator diameter demands reach the highest median value of 1160 mm, with upper and lower bounds of approximately 1550 mm and 700 mm, respectively, representing the widest distribution among all soil classes. This clearly demonstrates that isolation systems in softer soils require significantly larger isolator diameters to meet the higher base displacement demands associated with lower soil stiffness.

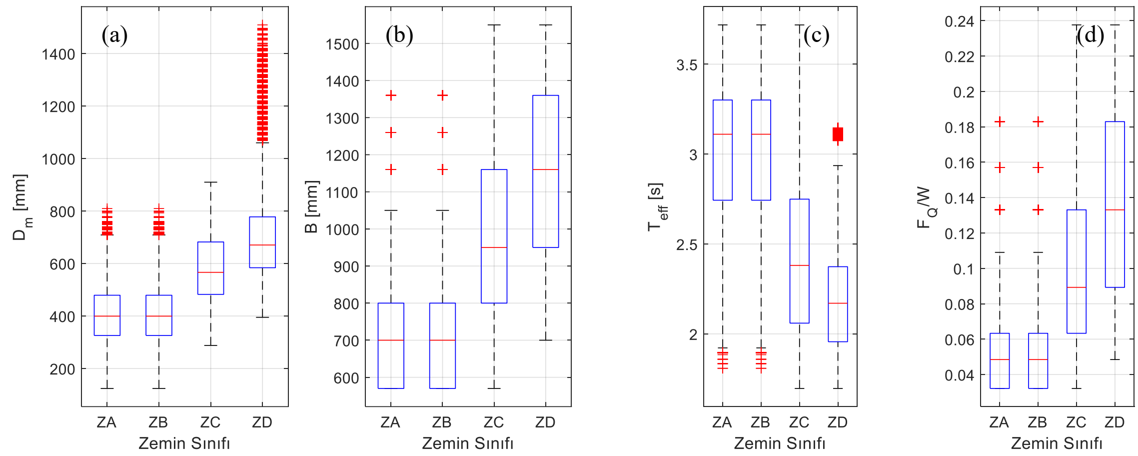

Fig. 4. Statistical distributions for soil classes ZA, ZB, ZC, and ZD: a) maximum base displacement, b) isolator diameter, c) effective period, d) characteristic strength ratio

In Fig. 4(c), the statistical distributions of the effective period (T_{eff}) values for different soil classes (ZA, ZB, ZC, ZD) are presented in boxplot format. For soil classes ZA and ZB, the median value is 3.1 s. The distribution range is relatively wide, with the lower quartile (Q1) around 2.7 s and the upper quartile (Q3) around 3.3 s. The upper and lower adjacent values are 3.7 s and 1.9 s, respectively. A few outliers are observed below the lower adjacent value (around 1.8-1.9 s). These low period values may result from stiffer isolation systems or design strategies aiming for smaller displacement demands. For the ZC soil class, the distribution range is considerably wider, with lower and upper adjacent values between 1.7 s and 3.7 s, and a median value of 2.4 s. Compared with the ZA and ZB soil classes, it exhibits significantly shorter periods. This reduction indicates that in stiff soils (ZC), the isolation system tends to be designed with shorter effective periods, or the relationship between displacement capacity and isolator diameter differs. For the ZD soil class, the median value is 2.17 s, representing the shortest effective period among all soil classes. The box height is relatively small, showing that the data are more uniformly distributed. The upper quartile value is 2.3 s, while a few outliers above the upper adjacent value (around 2.9 s) range between 3.07 s and 3.14 s. These upper outliers indicate that even in softer soils with lower stiffness, isolators may provide longer effective periods in regions with lower seismic hazard.

The statistical variation of the characteristic strength ratio (F_Q/W) for each soil class is illustrated in Fig. 4(d). For soil classes ZA and ZB, the median values are approximately 0.05, and the distribution ranges are relatively narrow. The upper quartile value is 0.06, while outliers above the upper adjacent value of 0.11 appear in the range of 0.13-0.18. These outliers indicate that even in stiff soil conditions, higher characteristic strength capacities may be required at locations near fault zones. For the ZC soil class, the median value increases to 0.09, the distribution becomes wider, and the upper quartile value reaches 0.13. The absence of outliers suggests that in stiff soils (ZC), the characteristic strength ratios (F_Q/W) are more uniformly distributed and do not exceed the statistical upper limits, even in areas close to fault lines. For the ZD soil class, the median value reaches the highest level at 0.13. The upper quartile value is 0.18, and the upper adjacent limit is around 0.24. The lack of outliers indicates that higher F_Q/W values are common design outcomes in soft soil conditions (ZD), reflecting a general trend rather than exceptional cases.

Fig. 5 presents the relationship between the effective period (T_{eff}) and base displacement demand (D_m) for the considered soil types. For the rock soil classes (ZA and ZB), as shown in Figures 5(a) and 5(b), the T_{eff} -D_m distribution indicates that in the short-period range (1.80-2.25 s), the Dm values vary between 560 mm and 810 mm. In the medium-period range (2.25-2.90 s), the displacement demands range from 420 mm to 650 mm. In the upper-medium period range (3.00-3.30 s), the D_m values vary between 305 mm and 460 mm. Moreover, in the period interval of approximately 2.90-3.80 s, a smooth characteristic trend is observed, showing that D_m increases proportionally with Teff depending on the isolator design parameters. In this range, the displacement demands vary between 120 mm and 360 mm. For the ZC soil class (Figure 5(c)), the base displacement demand varies between 650 mm and 910 mm within the short-period range (1.70-2.25 s). In the medium-period range (2.25-2.80 s), the demands decrease to approximately 430-650 mm, while in the upper-medium range (3.00-3.30 s), they remain between 305 mm and 460 mm. Additionally, for longer effective periods (3.60-3.70 s), the displacement demand slightly increases again, ranging from 287 mm to 360 mm. The ZD soil class exhibits base displacement demands of 610-820 mm in the short-period range (1.70-2.25 s). In another dataset within the same range, D_m increases from 820 mm to 1450 mm. This indicates that under relatively low-stiffness soil conditions, certain isolator configurations can lead to very high displacement demands at the initial periods. In the medium-period range (2.25-2.80 s), displacement demands vary between 425 mm and 710 mm, while in the upper-medium period range (2.80-3.20 s), D_m values are between 400 mm and 510 mm.

Fig. 6 presents the relationships between the characteristic strength ratio (F_Q/W) and the maximum base displacement (D_m) for different soil classes, taking into account the effective period (T_{eff}) values. In rock-type soils (ZA and ZB), the F_Q/W ratio ranges between 0.03 and 0.18, while the T_{eff} values vary from 1.7 s to 3.7 s. In this range, D_m values remain limited between 125 mm and 810 mm. For stiff soils (ZC), the F_Q/W ratio increases up to 0.23, and T_{eff} values show a wide distribution between 1.7 s and 3.7 s, resulting in D_m values reaching up to 910 mm. In softer soils (ZD), the F_Q/W ratio varies between 0.05 and 0.23, while T_{eff} values are distributed between 1.7 s and 3.1 s, and the corresponding D_m demands increase significantly, ranging from 390 mm to 1510 mm. These results indicate that the interaction between F_Q/W and T_{eff} directly influences displacement demands, and high displacement levels become critical under relatively low-stiffness soil conditions.

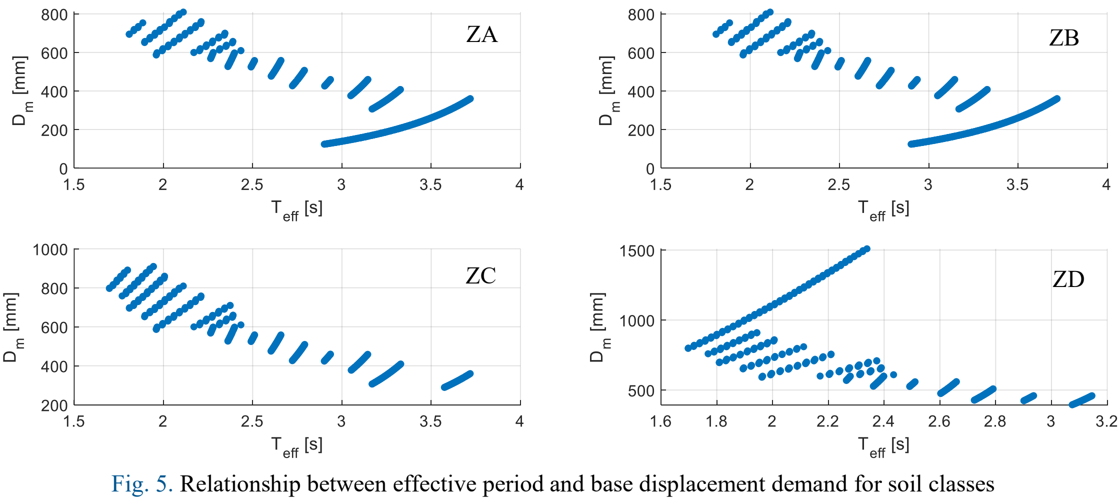

Fig. 5. Relationship between effective period and base displacement demand for soil classes

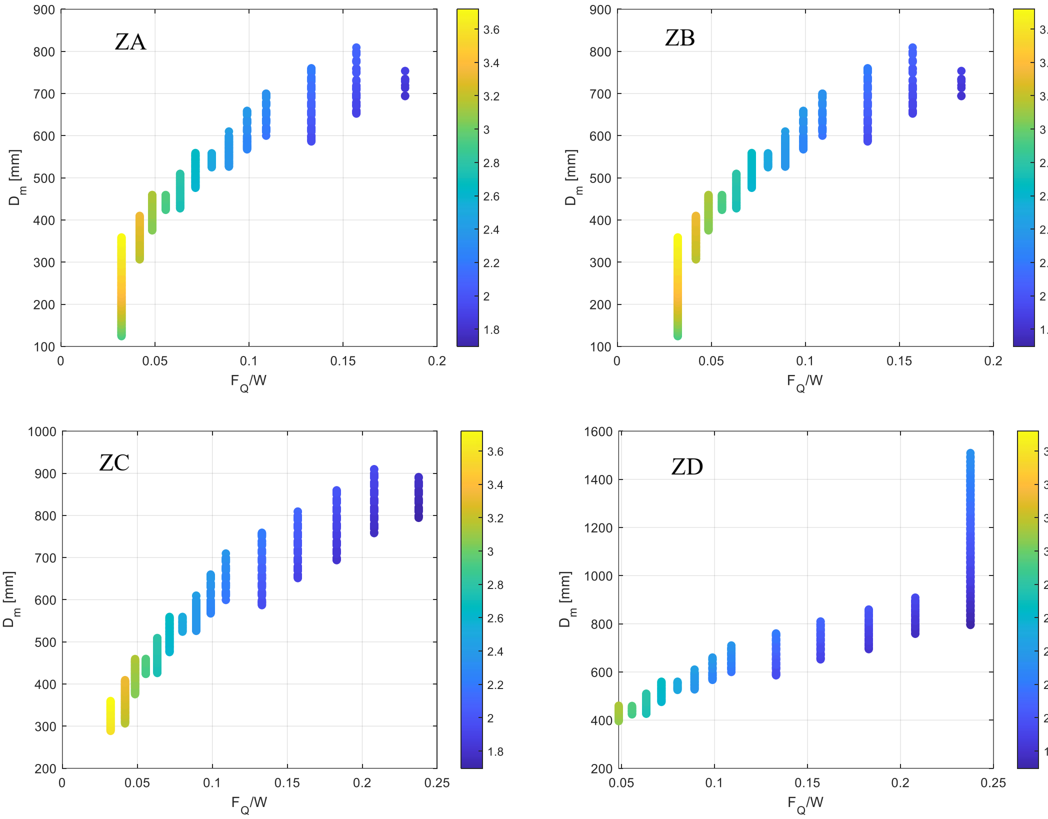

Fig. 6. Correlations between the characteristic strength ratio and the maximum base displacement for different soil classes. The color scale indicates the variation of the effective period (T_{eff})

In rock-type soils (ZA and ZB), the F_Q/W ratio varies between 0.02 and 0.18, while the effective period (T_{eff}) ranges from 2.0 s to 3.2 s. Under these conditions, the effective damping ratio (β_{eff}) is concentrated between 0.14 and 0.30, and an increase in the F_Q/W ratio corresponds to a noticeable decreasing trend in β_{eff} (Figure 7). This indicates that in rock-type soils, effective damping remains relatively high with limited variation. In stiff soils (ZC), the F_Q/W ratio increases up to 0.23, while T_{eff} values are widely distributed between 1.8 s and 3.6 s. In this case, βeff values remain within a narrow range of 0.14-0.23, showing a reduction in effective damping with increasing F_Q/W ratio. In the ZC class, β_{eff} values tend to cluster at higher levels for longer periods (3.0 s and above). This finding suggests that isolator configurations with longer periods and lower characteristic strength have an enhanced energy dissipation capacity. For soft soils (ZD), the F_Q/W ratio varies between 0.05 and 0.25, and T_{eff} values range from 1.8 s to 3.7 s. Under these conditions, β_{eff} values are concentrated within a narrow band of 0.15-0.19, showing a rapid and distinct decrease in damping ratio as the F_Q/W ratio increases.

As shown in Fig. 8, the maximum effective damping ratio (β_{eff}) in rock-type soils (ZA and ZB) is about 0.24, while in stiff (ZC) and soft (ZD) soils, β_{eff} decreases from approximately 0.23 to 0.19. In all soil types, when the base displacement exceeds around 600 mm, β_{eff} reaches its lowest values, whereas it increases noticeably when the displacement falls below 600 mm. At the same time, the increase in the effective period (T_{eff}) occurs concurrently with higher damping capacity, contributing to a more efficient performance of the isolation system.

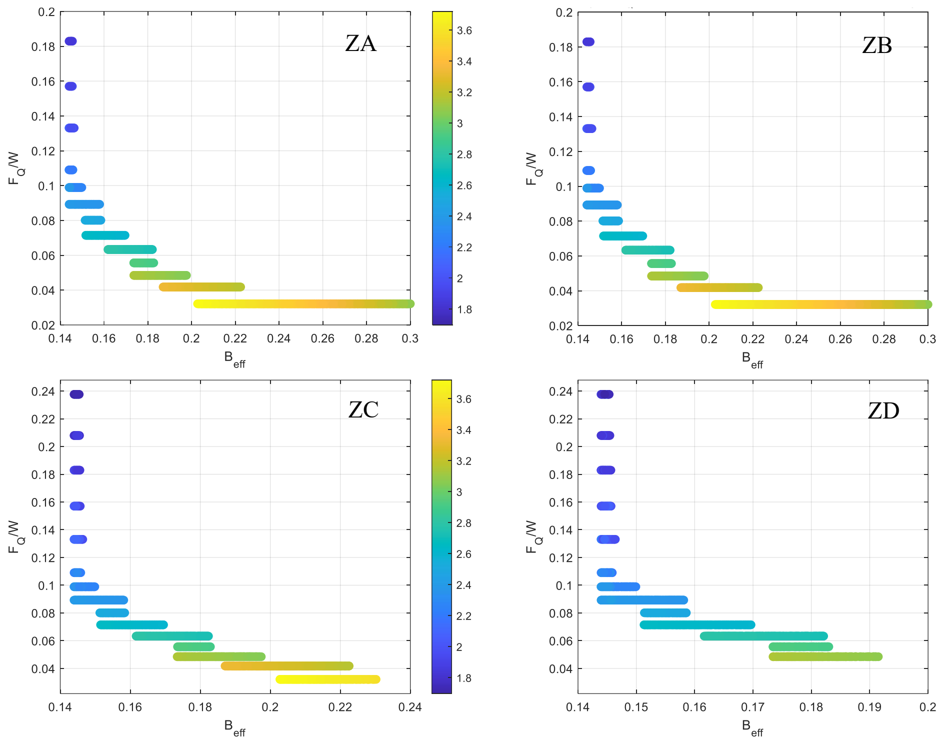

Fig. 7. Relationships between characteristic strength ratio and effective damping ratio for different soil classes. The color scale indicates the variation of the effective period (T_{eff})

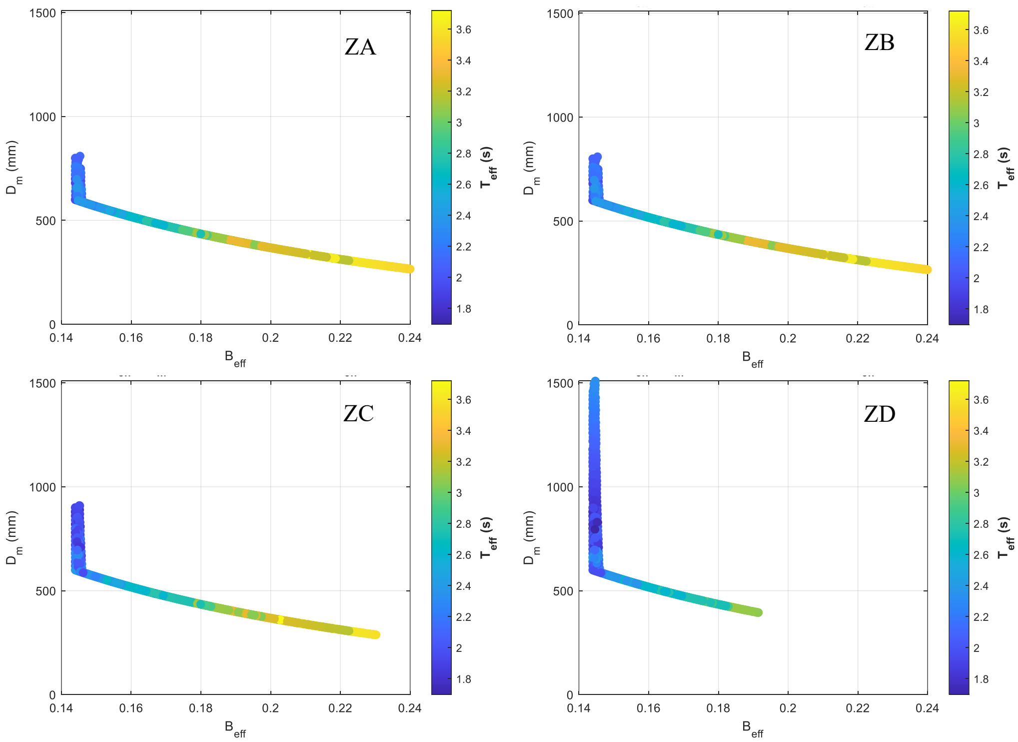

Fig. 8. Relationships between maximum base displacement and effective damping ratio for different soil classes. The color scale indicates the variation of the effective period (T_{eff})

3. Conclusions

This study presents a preliminary design-based evaluation of a seismic isolation system for a typical five-story reinforced concrete building equipped with lead rubber bearings (LRBs), considering all geographical coordinates in the Turkish Earthquake Hazard Map. Within this framework, key design parameters such as base displacement, isolator diameter, effective period, characteristic strength ratio, and effective damping ratio were statistically analyzed for soil classes ZA, ZB, ZC, and ZD. The main findings are summarized below to provide an order-of-magnitude reference for engineering design and applications.

- The median base displacement increases from about 400 mm in rock-type soils (ZA, ZB) to 566 mm in ZC and 670 mm in ZD. Maximum displacement demands reach 910 mm for ZC and up to 1500 mm for ZD. In particular, extreme displacements exceeding 1.0 m in ZD soils near fault zones cannot be mitigated only by increasing isolator size, and such conditions also make the design of seismic gaps physically difficult.
- The median isolator diameter increases from 700 mm in ZA-ZB to 950 mm in ZC and 1160 mm in ZD, with a maximum of about 1550 mm. These larger diameters occur locally in ZC soils but are more widespread in ZD soils, making the design process more demanding and costly.
- Isolation systems in ZA-ZB soils exhibit longer effective periods, with a median of 3.1 s, while ZC and ZD soils show shorter periods of 2.4 s and 2.17 s, respectively. This trend indicates that as soil stiffness decreases, isolation systems are designed for shorter periods. However, even with this design approach, extreme base displacements of up to 1.5 m can still occur near fault zones.
- The characteristic strength ratio (F_Q/W) generally increases from 0.05 in ZA-ZB soils to 0.09 in ZC and 0.13 in ZD. The highest values (0.23-0.24) are observed in ZC and ZD soils, confirming the need for higher strength capacities to meet increased displacement demands, particularly in soft soils.
- The effective damping ratio (β_{eff}) varies between 0.14 and 0.30 in ZA-ZB soils, remaining relatively high but showing a decreasing trend as F_Q/W increases. In ZC soils, β_{eff} ranges between 0.14 and 0.23 and increases when the effective period exceeds 3.0 s, indicating greater energy dissipation for long-period, low-strength isolators. In ZD soils, β_{eff} is limited to a narrow band of 0.15-0.19 and decreases rapidly with higher F_Q/W ratios, showing that damping capacity becomes restricted in lower-strength soils.
- The overall damping capacity remains around 20% in stiff (ZC) and soft (ZD) soils. Therefore, integrating additional damping devices could help reduce excessive displacement demands in ZC soils and prevent base displacements in ZD soils from exceeding physical limits, particularly near fault zones.
- In all soil classes, effective damping decreases when base displacements exceed 600 mm and increases when they fall below this level, revealing the close interaction between displacement and damping. Moreover, longer effective periods are associated with higher damping capacity, contributing to improved isolation performance.
- Although extending the effective period enhances energy dissipation and isolation efficiency, this goal is limited by physical constraints. The effective period depends on the characteristic strength (related to lead core area and yield shear stress) and on post-yield stiffness parameters such as the shear modulus, total rubber thickness, and rubber area. Consequently, geometric and material limitations make period extension and isolation system design a challenging engineering process.

Future research will aim to extend the proposed methodology to buildings with varying numbers of stories and different structural systems. Comparative investigations incorporating alternative isolation technologies (e.g., friction pendulum system and high-damping rubber bearing), near-fault effects, and nonlinear time-history analyses are also planned within the context of final design to provide a more comprehensive evaluation of seismic performance.

Declaration of conflicting interests

The author(s) declared no potential conflicts of interest with respect to the research, authorship, and/or publication of this article.

Funding

No funding was received for this study.

Data availability statement

The data that support the findings of this study are available from the corresponding author upon reasonable request.

References

[1] Alhan C, Hacıemiroğlu M (2023) Dirençli şehirler için depreme dayanıklı yapı tasarımında sismik izolasyon. Çevre Şehir İklim Derg 2(4):96–127.
[2] Skinner RI, Robinson WH, McVerry GH (1993) An Introduction to Seismic Isolation. John Wiley & Sons, Chichester.
[3] Naeim F, Kelly JM (1999) Design of Seismic Isolated Structures: From Theory to Practice. John Wiley & Sons, New York.
[4] Erdik M, Ülker Ö, Şadan B, Tüzün C (2018) Seismic isolation code developments and significant applications in Türkiye. Soil Dyn Earthq Eng 115:413–437. https://doi.org/10.1016/j.soildyn.2018.09.009.
[5] Kıral A, Gürbüz A (2024) Using supplemental linear viscous dampers for experimentally verified base-isolated building: Case study. J Struct Eng Appl Mech 7(1):34–50. https://doi.org/10.31462/jseam.2024.01034050.
[6] Komodromos P (2000) Seismic Isolation for Earthquake-Resistant Structures. WIT Press, Southampton.
[7] Alhan C, Öncü-Davas S (2016) Performance limits of seismically isolated buildings under near-field earthquakes. Eng Struct 116:83–94. https://doi.org/10.1016/j.engstruct.2016.02.043.
[8] Erdik MO (2017) State of the art on application, R&D and design rules for seismic isolation and energy dissipation for buildings, bridges and viaducts, cultural heritage and chemical plants in Türkiye. In: Proceedings of the 2017 NZSEE Conference. Wellington, New Zealand.
[9] ENR (2025) The 10 largest base-isolated buildings in the world. https://www.enr.com/articles/42366-the-10-largest-base-isolated-buildings-in-the-world. Accessed 10 Apr 2025.
[10] Şadan B (2022) State of the art in application of seismic isolation and energy dissipation in Türkiye. In: World Conference on Seismic Isolation. Springer, Cham, pp. 17–25. https://doi.org/10.1007/978-3-031-15696-9_2.
[11] TBDY (2018) Türkiye Bina Deprem Yönetmeliği. T.C. İçişleri Bakanlığı, Afet ve Acil Durum Yönetimi Başkanlığı, Ankara.
[12] Castaldo P, Ripani M (2016) Optimal design of friction pendulum system properties for isolated structures considering different soil conditions. Soil Dyn Earthq Eng 90:74–87. https://doi.org/10.1016/j.soildyn.2016.08.020.
[13] Hassan A, Pal S (2018) Effect of soil condition on seismic response of isolated base buildings. Int J Adv Struct Eng 10(3):249–261. https://doi.org/10.1007/s40091-018-0204-5.
[14] Cheshmehkaboodi N, Guizani L (2021) On the influence of earthquakes and soil characteristics on seismic response and performance of isolated bridges. Arab J Geosci 14:640. https://doi.org/10.1007/s12517-021-06451-6.
[15] Kömür MA, Deneme İÖ, Oruç R (2019) Seismic response of fixed-base and LRB base-isolated RC frame systems under near-fault and far-fault excitations. J Struct Eng Appl Mech 2(4):174–189. https://doi.org/10.31462/jseam.2019.04174189.

[16] Yanik A, Ulus Y (2023) Soil–structure interaction consideration for base isolated structures under earthquake excitation. Buildings 13(4):915. https://doi.org/10.3390/buildings13040915.

[17] Ghosh S, Das D (2024) Seismic response of base-isolated buildings under near-field and far-field earthquakes considering SSI. In: IOP Conf Ser Earth Environ Sci 1326:012020. https://doi.org/10.1088/1755-1315/1326/1/012020.

[18] AFAD (2018) Türkiye Deprem Tehlike Haritası (TDTH) Platformu. https://tdth.afad.gov.tr. Accessed 20 May 2025.

[19] The MathWorks Inc. (2025) MATLAB: The Language of Technical Computing, Version 2023a. Natick, MA. https://www.mathworks.com.

[20] QGIS Development Team (2025) QGIS Geographic Information System, Version 3.40.7. Open Source Geospatial Foundation Project. https://qgis.org.

[21] Dynamic Isolation Systems. https://www.dis-inc.com.

[22] Whittaker AS, Sollogoub P, Kim MK (2018) Seismic isolation of nuclear power plants: past, present and future. Nucl Eng Des 338:290–299. https://doi.org/10.1016/j.nucengdes.2018.08.012.